5-2009

Electrostatic Discharge in Spacecraft Materials

Jennifer Roth
Utah State University

JR Dennison
Utah State Univesity

Ryan C. Hoffman
Air Force Research Laoratory

David Peak
david.peak@usu.edu

ELECTROSTATIC DISCHARGE IN SPACECRAFT MATERIALS

by

Jennifer Albretsen Roth

Thesis submitted in partial fulfillment of the requirements for the degree

of

HONORS IN UNIVERSITY STUDIES WITH DEPARTMENTAL HONORS

in

Physics in the Department of Physics

Approved:

Thesis/Project Advisor	**Departmental Honors Advisor**
Dr. J.R. Dennison	Dr. David Peak

Director of Honors Program
Dr. Christie Fox

UTAH STATE UNIVERSITY
Logan, UT

May 2009

ABSTRACT

Electrostatic Discharge in Spacecraft Materials

by

Jennifer A. Roth, Bachelor of Science

Utah State University, 2009

Faculty Mentor: Dr. J. R. Dennison
Graduate Mentor: Ryan Hoffmann

Understanding the characteristics of electron beam bombardment that induce electrostatic discharge (ESD) of insulating materials is crucial to constructing an electrically stable spacecraft. A measurement system has been designed to determine the beam energy and charge flux densities at which typical spacecraft materials intended for the James Webb Space Telescope (JWST) undergo ESD. Because discharge events occur over time intervals ranging from nanoseconds to minutes, multiple detection methods were employed as charge was accumulated on a sample surface; these methods included monitoring of sample current and optical emissions from the sample surface. Each sample was also examined with optical microscopy before and after testing to determine permanent changes in the materials. Testing for various samples was done at 130 K, 170 K, and 200 K.

An overview of ESD incidence for all materials is provided in relation to beam conditions and material composition. Data for a carbon fiber material is discussed in greater detail, comparing results from each detection method. Two discharge modes were observed: a sudden-onset, long-duration exponentially-decaying sample current accompanied by the release of intense blue photons, and a sudden spike or arc in current with a white light flash. The implications of test results for JWST are discussed.

ACKNOWLEDGEMENTS

This thesis would not exist without the support of several influential people. Thank you to Dr. J.R. Dennison, my amazing faculty mentor of over two and a half years. He has given me the chance to be involved in surface physics projects, encouraged me to attend professional meetings, and has always made sure that I not only perform experiments, but learn physics as I do so. I am also very grateful for the mentorship of Ryan Hoffmann, who has spent hours over the last few years teaching me everything from the definition of a secondary electron to how to use a socket wrench. Also, thank you to Jonathan Tippets, for solving my computer woes and for collaborating with J.R., Ryan, and I on the ESD study. Thanks to everyone in the surface physics group (Justin Dekany, Amberly Evans, Jesse Hayes, Josh Hodges, Alec Sim, Charlie Sim) who have all played some role in this laborious ESD study. I would also like to thank Dr. David Peak for encouraging me to pursue research, fellowships, and scholarships, and for serving on my honors thesis committee.

I have been blessed with supportive family and friends who have helped me on the road to this degree. I am so grateful for Tamara Jeppson, a brilliant study companion and a true friend. Thank you to my Aggie sisters, Angela Albretsen for helping me adjust to college life my freshman year, and Emily Albretsen for bringing so much enthusiasm and laughter to my senior year. I am grateful to my grandparents, Keith and Carol Checketts, who provided me not just a house to live in for three years, but also love and encouragement. My paternal grandparents, Connie and Bruce Albretsen, have also actively supported me in my educational and other pursuits and I am grateful for their love. I have incredible parents, Jay and Mary Albretsen, who have always supported my personal and educational goals. I would certainly not be where I am today without their love and encouragement. Thank you to Ruth Harrison, my aunt and friend, who has provided sound advice and assistance throughout my years at USU. Finally, I would like to thank my husband, Gable Roth. Whether you were fixing me dinner after a long day, being a sounding box for my ideas, making me laugh when I was stressed, or encouraging me to keep moving forward, you have given me strength to write this thesis.

CONTENTS

LIST OF FIGURES

LIST OF TABLES

CHAPTER 1

INTRODUCTION

Though many never think about what happens above ground level, everyone is impacted by satellites—from the business executive in a bustling city to the flood victim in a remote village. Practical applications of satellite technology include accurate mapping, weather forecasting, natural disaster response, global positioning, communications, and myriad scientific research applications for geology, atmospheric science, physics, astronomy, ecology, and other fields. One of the most famous satellites designed for scientific purposes is the Hubble Space Telescope. Launched in 1990, the Hubble has produced astronomical images of immense scientific value and breathtaking beauty, observing even young galaxies formed not long after the Big Bang.[1] A new orbiting telescope is now being designed that will observe radiation in the infrared and near-infrared range.

NASA, in conjunction with the European (ESA) and Canadian (CSA) Space Agencies, is designing and constructing this next generation space telescope, called the James Webb Space Telescope (JWST). It is scheduled to launch in 2013 and to make observations for at least 10 years. The craft will reside at the second earth-sun Lagrange point (L2), where it will orbit the sun at the same rate as the earth, permanently shielded from the sun by earth's shadow.[2] At this location, the telescope will operate at a temperature less than 40 K.[3]

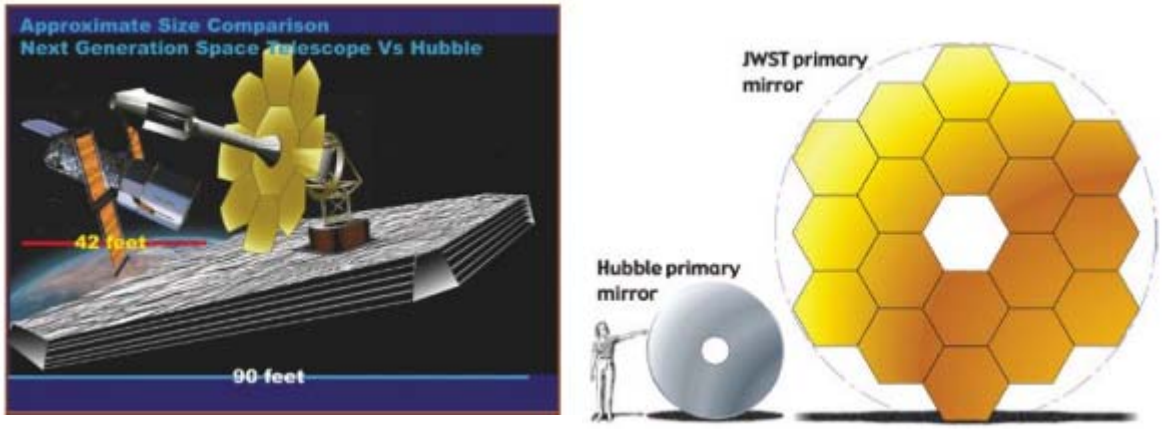

Fig 1.1: Size comparisons of the Hubble Space Telescope and the James Webb Space Telescope.[4]

The JWST consists of a telescope, an IR and near-IR instrument package, sunshield, and spacecraft. Larger than Hubble (4.2 m x 13.3 m), the spacecraft is approximately 12 m by 22 m.[4] Its primary mirror is approximately 6.6 m in diameter and consists of 18 hexagonal beryllium components.[3] This telescope is intended to study four main topics: first light and reionization, the assembly of galaxies, the evolution of stars, and planetary systems and the origins of life.[3]

Materials for the craft were selected to withstand the conditions and constraints of the JWST mission. For instance, in order to fit inside a rocket for launching, the JWST is able to "fold up" into a 16.3 m by 4.75 m rectangle.[4] The craft must also be able to function at the low temperature and, as is the focus of this study, be able to operate in the electrically charged space plasma environment.

Satellites, especially JWST, are expensive to design, build, and launch, and are often impossible to repair. Therefore, it is vital that these craft be created to withstand the conditions of the space plasma environment in which they reside. It is particularly important to mitigate the effects of electrical charging, which accounts for more than half of spacecraft anomalies attributed to space environment interactions.[5] Without other means of dissipating built-up charge, electrostatic discharge (ESD) can occur, causing anomalies ranging from circuit malfunctions to material destruction. The purpose of this study is to understand electron-induced electrostatic discharge for JWST materials, in order to ensure the electrical stability of the spacecraft. Results can also improve the understanding of ESD theory and the occurrence of ESD in similar materials used for both space and ground applications.

CHAPTER 2

THEORY

This section provides brief explanations of spacecraft charging and several phenomena that may occur when materials are brought into contact with high energy electrons. These explanations prove very useful when analyzing ESD data.

2.1 Spacecraft Charging

In order for satellites to function they must be designed to withstand the conditions of the space plasma environment. This plasma is composed of photons, ions, and electrons that interact electrically with the surfaces of spacecraft, as shown in Figure 2.1. Of these energetic particles, electrons are the largest contributor to spacecraft charging, due to their high mobility.[6] Electron interactions will be the focus of this study.

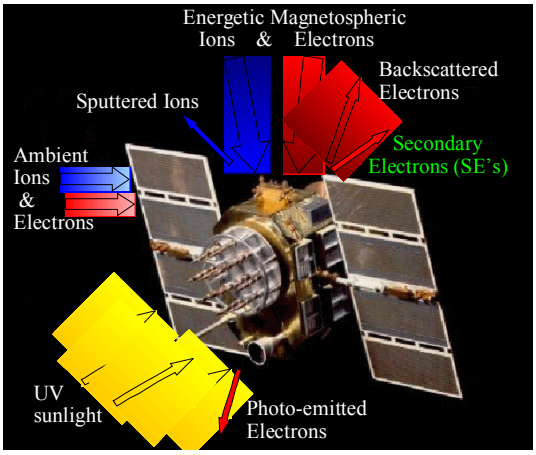

Fig. 2.1: Illustration of electrical interactions between a satellite and the space plasma environment.

The typical low-energy plasma environment for satellites in L2 orbit is created by ambient solar wind, the magnetosheath and the magnetotail.[7] The energies of incident electrons in this environment range from about 10 eV – 1 keV.[7] When solar storms arise, the L2 environment becomes populated with higher energy particles, ranging from about 10 keV – 1 MeV.[7] As the spacecraft surface interacts with these electrons, the once electrically neutral material becomes charged. The energy and flux of impingent electrons and the resistivity of the material determine the amount of charge accumulated.

2.2 Conduction vs. Accumulation of Electric Charge

Charge accumulation, which is the forerunner to ESD, depends upon three key factors: the nature of incident electrons, the exposure time, and the electrical resistivity of the material. The energy distribution and flux density of incident electrons, as well as the time the material is exposed to the electrons, determine the magnitude of the charge and energy incident on the material. The conductivity of the material, which is temperature and material-dependent, determines how the material responds to this influx of charge.

For metals or conductors, which have high conductivity, this charge is conducted rapidly. On earth, the charge can be conducted to ground, and the material then returns to its electrically neutral state. However, metal surfaces in space are ungrounded, so the entire metal surface develops a voltage relative to the ambient plasma environment, a process known as absolute charging.[8] According to the semiclassical model of electron dynamics, the high mobility of electrons in metals or conductors results from the partially filled valence and conduction bands in these materials.[9] By a similar token, good insulators have low conductivity due to electron bands which are completely full or completely empty.[9] Because insulators are not able to conduct charge rapidly, an

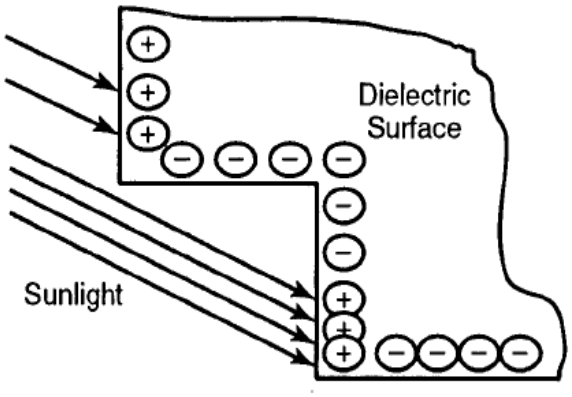

Fig. 2.2: Differential charging on a dielectric surface.

insulator will not likely have a constant voltage across its surface. Instead, regions of high and low voltage can develop—a process known as differential charging (See Figure 2.2).[8] Often differential charging occurs between regions that are shaded and regions in full sunlight as in Fig. 2.1B.[8] Voltage differences across the surface of a dielectric, or voltage differences between metal and insulating surfaces can cause ESD. This type of arc discharge, across surfaces, is known as "flashover" discharge.[10]

Deep dielectric or bulk charging can also lead to ESD. Bulk charging occurs in dielectric/insulating materials or on insulated floating conductors as energetic electrons are deposited in a material.[8] If electrons are deposited at a faster rate than they are dissipated, an electric field develops in the material. If this electric field becomes larger than the breakdown strength, arc discharging occurs through the material, an ESD event known as "punch-through" discharge.[8, 10]

In some cases, discharges can also occur from a spacecraft to ambient space plasma, a phenomena known as "discharge to space."[10] This occurs when the craft develops a large electric potential relative to the ambient plasma.

2.3 Continuous Slow-Down Approximation

The continuous slow-down approximation (CSDA) is a useful model for deep dielectric charging. The CSDA assumes that an electron loses its energy at a constant rate as it moves through a material.[11] Under this model, an electron will eventually lose all of its energy and will be deposited at some range, R. As time passes, charge is accumulated thereby producing a sample voltage, V_S, which obeys the following relation for a plane of charge,

$$V_S = J_B \cdot t \cdot R/(2\varepsilon_0), \qquad (1)$$

where J_B is the current density of the electron beam and t is the exposure time of the sample to the electron beam.[12] When this voltage reaches the material-dependent breakdown voltage, ESD can occur.

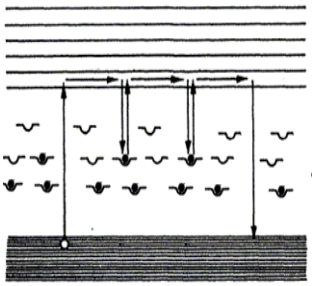

Fig 2.3: Illustration of Radiation Induced Conductivity. Black dots represent electrons.

2.4 Radiation-Induced Conductivity

Another factor that affects the dissipation of charge in a material is Radiation Induced Conductivity (RIC). This occurs when radiation of sufficient energy to overcome a

band gap excites electrons into the conduction band. These electrons travel some distance before decaying to a localized intermediate trapped state, where they can easily be excited back into the conduction band. This pattern repeats itself until the electron decays back to its ground state, as in Figure 2.3.[13]

It is possible that RIC could play a significant role in conduction during tests with high energy electron beam radiation, such as the experiments performed in this study.

2.5 Luminescence

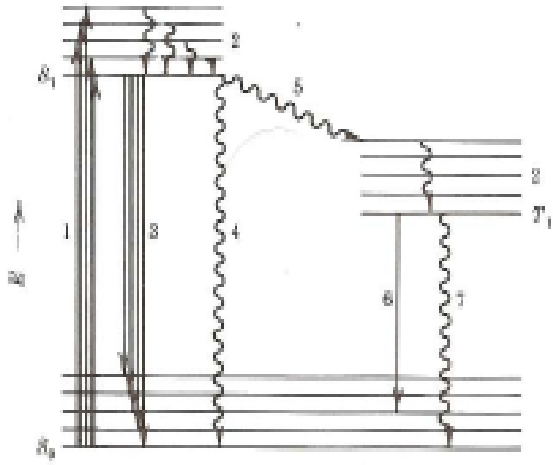

Fig 2.4: Illustration of luminescence. After decaying to an intermediate state, an electron decays to a lower state, and a photon is emitted.

In a similar manner, luminescence can occur when a quantum of radiation excites an electron into the conduction band.[14] Instead of moving back and forth between an intermediate state and the conduction band as in RIC, luminescence occurs when electrons decay from the intermediate trapped state to a lower state, releasing photons in the process, as in Figure 2.4. Luminescence occurs over time intervals ranging from 10's of nanoseconds to 10's of seconds. This is another phenomenon that could occur during high energy electron beam irradiation.

CHAPTER 3
METHODS

3.1 Experimental Set-up

Various techniques were used to simulate the environments to which the JWST will be exposed, to induce arcing, and to detect arcs. First, samples were prepared to fit on 1-cm diameter cylindrical copper billets. These were placed in a sample carousel, which was housed in the USU Electron Emission Chamber, an ultra high vacuum (UHV) chamber. A vacuum pressure of about 10^{-8} to 10^{-9} Torr was maintained in order to eliminate atmospheric charging and absorption effects, and to approach the low atomic pressures of the space environment.

Tests were performed at three temperatures: 130 K, 170 K, and 200 K. In order to maintain these temperatures, the sample stage was cooled using liquid nitrogen. The flow of liquid nitrogen was regulated by a temperature controller. Although the JWST will be submitted to much lower temperatures, the low temperatures used in experimentation provide useful information about the effect of temperature on ESD occurrence. It was expected that temperature changes would affect electrostatic discharge events, since the resistivity of a given material is temperature-dependent.

In space, a satellite will be exposed to a certain flux of electrons over a number of years. In the laboratory, it would be impractical and expensive to submit samples to an extremely low-flux electron beam over a time scale of years. Instead, the sample is exposed to similar amounts of total charge by decreasing the exposure time and increasing the electron flux. Samples were exposed to an electron beam from a High Energy Electron Diffraction (HEED) gun. The electron beam had current densities of 0.1 nA/cm^2 and 1.0 nA/cm^2, and energies equal to 22 keV or 7 keV for total exposure times 1000 s and 3600 s. Before each run, the HEED gun was conditioned to the appropriate beam energy and spot size (large enough to cover the entire 1-cm diameter sample area.) The beam was then directed at a Faraday cup and adjusted until the appropriate current density was obtained.

Before experimentation began, several measurements were taken to characterize the HEED beam. The HEED gun was condition to a specific energy, defocused, and then swept over a standard Faraday cup. Current measured from the Faraday cup was deconvoluded to determine the size and shape (Gaussian) of the beam. This was done to determine the current density of the beam at various energies, and to ensure that the beam would cover the entire surface of each 1-cm diameter sample.

All of these initial experimental conditions were met in order to minimize atmospheric effects and approach the conditions of the space plasma environment to which the JWST will be subjected.

3.2 Detection Methods

Although models of space plasma arcing can be useful, actually performing arc testing is imperative to understanding the reaction of a material to the space plasma environment.

This is because phenomena not predicted in arc models often occur in actual ESD testing.[15] ESD events can occur over time intervals ranging from picoseconds to microseconds.[16] Peak currents of ESD phenomena also have a wide range, from milliamps to tens of amps.[16] Because of their highly unpredictable nature, several measurement techniques were used to detect and characterize ESD events. As the electron beam was irradiating the sample surface, a still camera and video camera were positioned to observe the sample surface. A wire connected to the back of the sample billet allowed current to flow through a Resistor, and Pearson Coil. The current flowing through these devices was measured by an oscilloscope. Sample current was also measured by a feedback ammeter or electrometer. By using a variety of capture devices of different sensitivities, a wide range of optical and electrical data was obtained.

Induced Electrostatic Breakdown Test Resolutions

Property	Units	Current Tests			Image Tests		
		Oscilloscope Resistivity	Oscilloscope Pearson Coil	Electrometer	Low Light Video	High Res. Still	Microscope Before/After
Temporal Resolution	msec	$\sim 5 \cdot 10^{-4}$	$\sim 5 \cdot 10^{-4}$	18	33	34,600	NA
Test Duration	sec	$\sim 2.5 \cdot 10^{-2}$	$\sim 2.5 \cdot 10^{-2}$	Full Test	Full Test	30	NA
Spatial Resolution	µm/Pixel	NA	NA	NA	59	55	10
Image Size	µm Pixels	NA	NA	NA	18900x14200 640x480	14500x13900 265x255	10000 5725
Spatial Conversion Factor	µm/Pixel	NA	NA	NA	29.5	54.6	1.75
Energy Resolution	µJ/ Pixel-Count	$\sim 2 \cdot 10^{-3}$	$\sim 2 \cdot 10^{-3}$	$\sim 2 \cdot 10^{-4}$	55	105	NA
Maximum Energy	µJ	~4	~6	~5	~4 µJ ~13 µJ/Pixel	~1.7 µJ ~25 µJ/Pixel	NA
Energy Conversion Factor	varies	NA	NA	0.18 J/A	~0.05 µJ/Pixel-Count	~0.01µJ/Pixel-Count	NA
Wavelength Resolution	---	NA	NA	NA	RGB	RGB	Full Color

Table 3.1: Instrument Test Resolutions for ESD experiments.

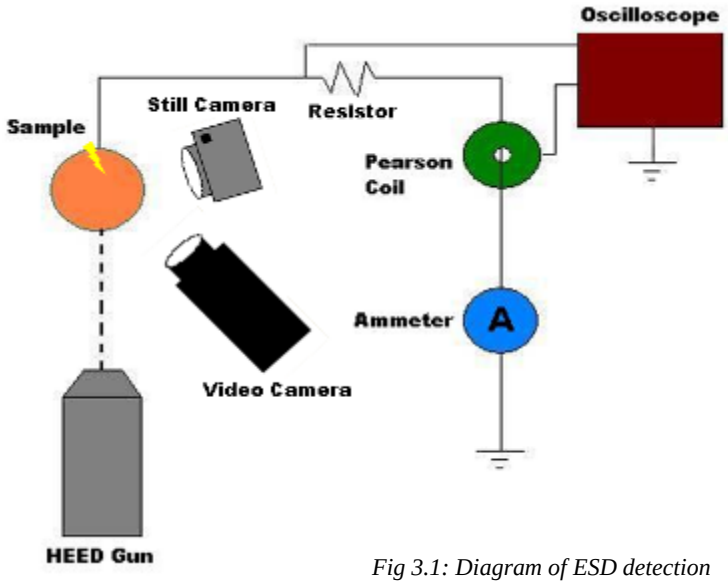

Fig 3.1: Diagram of ESD detection

3.2.1 Pearson Coil

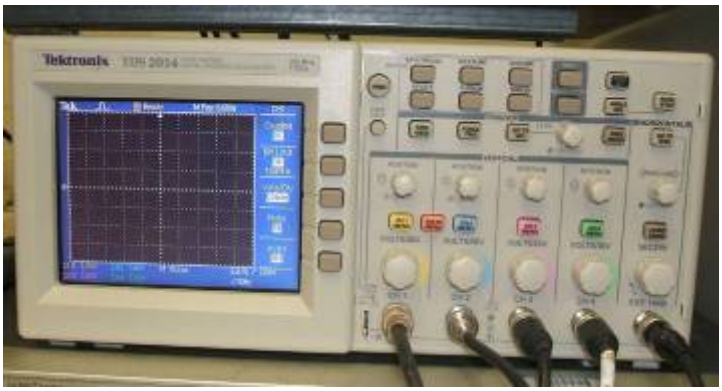

Fig 3.2: Tektronix TDS 2014 Digital Storage Oscilloscope—measures Pearson Coil, resistor current data.

Fig 3.3: Pearson Electronics Current Monitor.

One of the current measurement methods uses a Pearson Electronics current monitor, also known as a current transformer or Pearson Coil. The sample current passes through the center of the Pearson Coil, which then outputs 0.1 V for every 1A of sample current. If the sample current detected by the Pearson Coil rises above a user-defined threshold a Tektronix TDS 2040 Digital Storage Oscilloscope records a user-defined time interval of data about the trigger event. The time between data points depends upon this user defined time-interval. For most experiments, the time between data points was 2 ns.

The current recorded by the Pearson Coil contains a high level of noise. As the transformer is very sensitive, it detects other nearby current sources. Often it is difficult to separate the sample current from all of the stray currents appearing in the data. Although this measurement technique does have this disadvantage, it also has a major advantage. It has a greater sensitivity and a faster response time than the resistor technique.

3.2.2 Resistor/Shunt Ammeter

Another device used for measuring current is a shunt ammeter, made with a 47-ohm resistor. The oscilloscope also acts as the voltage meter for this method. Ohm's law states that the voltage drop (V) across the resistor is the product of the current passing through the resistor (I) times the resistor value (R),

$$V = I \cdot R \qquad (2)$$

Current from the sample, or input current (I_{in}), flows through a resistor, known as the shunt resistor (R_{sh}). The shunt ammeter measures the voltage drop, or output voltage (V_o), across the shunt resistor. The current is calculated by using Ohm's law, as in the equation (3).

$$I_{in} = V_o / R_{sh} \qquad (3)$$

A major advantage of using this measurement technique is the high current resolution (i.e. less noise from stray current sources), especially when compared with the magnitude of the noise in the Pearson Coil data. In some cases, this measurement method provides current data when the signal from the Pearson Coil is buried in the noise.

One disadvantage to this method of current measurement is the slower response due to a time constant delay,

$$\tau = R_{sh}C_o \qquad (4)$$

where C_o is the capacitance of the system.[17]

3.2.3 Electrometer/ Isolation amplifier board

A third technique for measuring current uses the electrometer/isolation amplifier board built by Dr. J.R. Dennison. The electrometer has a sampling rate of approximately 60 Hz. Unlike the current data for the oscilloscope, which is only recorded when triggered, the electrometer current data is recorded for the entire duration of each experiment.

3.2.4 Optical Microscope

This is the only optical measurement not recorded during ESD testing. Images of each sample surface are taken before and after ESD testing. A Canon Rebel XT Digital SLR camera is connected to a Zeiss microscope at 2.5X magnification. Photographs are taken over the entire sample surface, and are then stitched together in Photoshop. Each image has a pixel resolution of 1.70 μm/pixel.

The images before and after are carefully reviewed and compared with one another, and notes are made of any differences between the two. Particular attention is devoted to detecting scorch marks and other physical signs that suggest the occurrence of an ESD event. The location and magnitude of these markings are recorded.

Fig 3.4: Zeiss Optical Microscope.

3.2.5 Low-level Video Camera

Footage of the sample as it was irradiated was taken by a Xybion low-level light video camera, which is sensitive into the near infrared range. The camera resided outside the vacuum chamber, and observed the sample through a quartz window. This video stream was recorded onto videotapes using a Sony camcorder at a rate of approximately 30 frames per second. The video was converted to AVI format for digital storage and to aid in analysis.

Each video was viewed twice, looking for flashes indicative of an ESD event. The times at which flashes appear in the video were compared with the times at which events occurred in the current data.

The video is recorded in grayscale/black and white. Although it lacks spectral data, it does indicate the magnitude of photons released during arcing. The video data is also advantageous in that it is an optical data set with timing information of about 30 ms, which information is not contained in the other two optical analysis methods.

3.2.6 Digital SLR Camera

Still photographs of each sample were taken during ESD testing using a Canon Rebel XT Digital SLR camera. As with the video camera, the still camera was placed outside of the vacuum chamber and focused on the sample through a quartz window. The camera shutter was opened to download the image for 30 seconds and closed for four seconds of reset time. This pattern was repeated for the duration of the experiment. For every experiment, photographs were converted to bitmap images and cropped identically. These images were analyzed using a MathCad program that determined the intensity of the red, green, and blue light as well as the total light intensity of each frame.

Fig 3.5: Canon Digital SLR Camera

Although this optical analysis method lacks precise timing information to indicate when arcs occurred, it does provide spectral information about the arcing in the visible range, and has a better spatial resolution than the video camera. The still photographs are also an excellent source for determining the locations on the sample surface at which ESD occurred.

3.3 Materials Tested

Tests were performed for four types of materials used as structural and optical/thermal materials for JWST. Tables 4.6 and 4.7 contain test results for each of these materials, and specify each material's test designation number. Detailed descriptions of each material follow.

3.3.1 M55 J Carbon Fiber Tube

The M55J Carbon fiber tube material consists of an approximately 3000 μm carbon composite layer with about 25 μm of an epoxy resin on top.[13] This material was tested in experiments 50, 51, 52, and 53 reported in Chapter 4.

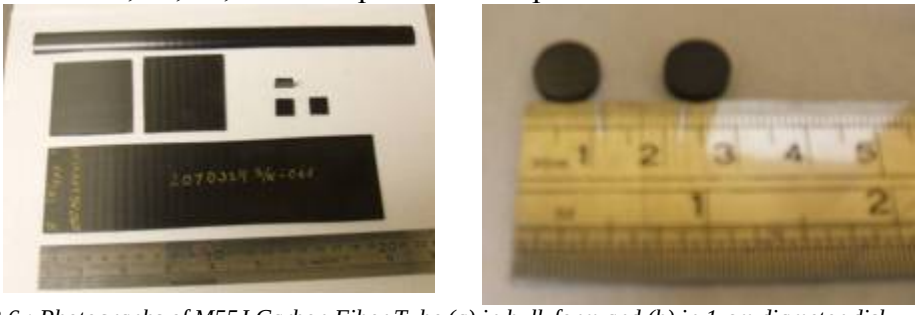

Fig 3.6.: Photographs of M55J Carbon Fiber Tube (a) in bulk form and (b) in 1-cm diameter disk.

3.3.2 IEC Radiator Reflector Material

The IEC Radiator Reflector Material, referred to as "IEC Au" elsewhere in the report, contains several layers. The top layer is ~ 0.1 μm gold (Au), followed by ~0.01 μm chromium (Cr). These metal layers are located atop 100 μm fiberglass/epoxy composite atop about 1000 μm carbon fiber composite, atop an additional 100 μm fiberglass/epoxy composite.[13] This material was tested in test 60, 61, and 62 reported in Chapter 4.

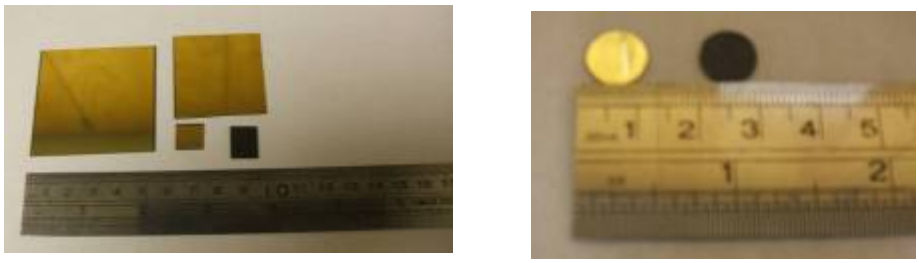

Fig 3.7: Photographs of IEC Radiator Reflector Material (a) in bulk form and (b) in 1-cm diameter disk.

3.3.3 IEC Shell Face Sheet with Carbon Veil

This IEC Shell Face material has a total thickness of approximately 1500 μm. One ply carbon fiber veil is situated atop six plies fiberglass all embedded in an epoxy resin material. Approximately 25 μm epoxy resin is layered on top of the carbon veil.[13] This material was tested in experiments 70, 71, 72, and 73.

3.3.4 Au Coated Fiberglass IEC Frame

The material consists of a fiberglass/epoxy composite coated with gold (Au) and chromium (Cr).[11] The sample, from top to bottom is approximately 0.1 μm Au on ~0.01 μm Cr, on a thin ~25 μm layer of epoxy resin, on about 100 μm E765/120 style fiberglass, on about 1500 μm of E765/7781 style fiberglass composite, on another 100 μm of E765/120 style fiberglass.[13] This material was used in tests 80, 81, and 82.

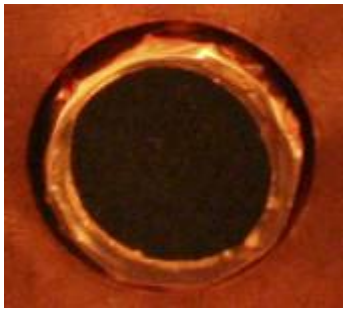

Fig 3.8: Photograph of IEC Shell Face Sheet with Carbon Veil mounted on copper billet. A Cu tape cap around the outside edge of the sample is used to ground the upper surface.

Fig 3.9: Photograph of Au Coated Fiberglass IEC Frame mounted on a copper billet. A Cu tape cap around the outside edge of the sample is used to ground the upper surface.

CHAPTER 4

DATA AND ANALYSIS

This chapter describes the results of the tests for the four materials described in Section 3.3. Section 4.1 provides an overview of results for all 14 experiments. Section 4.2 includes more in-depth analyses of all experiments for the IEC Shell Face Sheet material.

4.1 Overview for all materials

The results of all fourteen experiments performed for the four materials described in Section 3.3 are summarized in Tables 4.1 and 4.2 below. Two types of ESD events were observed. One type of discharge was an arc observed as a spike in current data or a flash in the optical data. The other discharge type was observed as a sudden-onset exponentially decaying current accompanied by a glow. Table 4.3 provides information about the occurrence of these glows in relation to the electron beam energy and current density.

ESD events were observed during three of the four experiments on M55J carbon fiber tube—Tests 50, 51, and 52. The experiment that had no arc events (Test 53) used the highest electron beam flux density, but was of shorter duration (1000 s) and had smaller beam energy (7 keV).

It is obvious that ESD occurred during Tests 60 and 61 for Au/Cr coated fiberglass, as arc events were detected by all six instruments. Glows occurred around the sample edge. Damage sites observed by ex-situ microscope imaging, and oscilloscope triggers during the experiment suggest arcing also occurred during Test 62. Sample damage incurred during experimentation included the removal of gold from the surface of the sample. By comparing grayscale bitmap images before and after experimentation, it was determined that approximately 2% of the Au surface area was removed during Test 61.[12]

For Test 70, which had the higher electron beam energy ($E_B = 22000 \pm 1$ eV) and the lower flux current density ($J_B = 0.1 \pm 0.1$ nA/cm^2), one persistent exponentially decaying current and one persistent exponentially growing current were seen as well as at least 35 arc events. Test 71 had the same beam energy and a higher current density ($J_B = 1.5 \pm 0.03$ nA/cm^2), but lasted only 1000 seconds. At least five arcs and one long decay were observed. Only one possible arc event was detected by the oscilloscope during Tests 72, which had the lowest electron beam energy, and current flux density. Test 73 had the lower energy, but the higher current flux density and lasted longer than Test 72. At least two arc events occurred, but no exponentially decaying currents were seen.

An exponentially-decaying glow was observed around the upper left edge of the samples during Tests 80 and 81. At least one arc event also occurred during both of these experiments. Three possible ESD events were detected only by the still camera during Test 82. None of the other data indicated that electrostatic discharge had occurred during this test, which had the lowest beam energy (7 keV) and a low current density ($J_B = 0.25 \pm 0.03$ nA/cm^2).

Induced Electrostatic Breakdown Test Results Overview

Test	Test Parameters	Current Tests			Image Tests			Summary
		Oscilloscope Resistance	Oscilloscope Pearson Coil	Electrometer	Low Light Video	High Res. Still	Microscope Before/After	
M55J carbon fiber tube for ISIM structure								
50	E_B=(22000±1) eV J_B=(0.125±0.004) nA/cm^2 Duration=(3600±3) s T=(133±2) K	Arc Observed	Arc Observed	3 Exponential Decays	1 Arc 2 Glows	1 Arc 2 Glows	2 Large Features	2 small arc early. 2 large events resulting in visible damage and blue fluorescence. Excellent coincidence.
51	E_B=(22000±1) eV J_B=(0.99±0.02) nA/cm^2 Duration=(1000±3) s T=(133±1) K	Arc Observed	Arc Observed	1 Exponential Decays 2 Spikes	1 Long Arc 1 Glow	1 Glow	2 Small Features	2 medium events resulting in visible damage and blue fluorescence. Good coincidence.
52	E_B=(7000±1) eV J_B=(0.10±0.01) nA/cm^2 Duration=(3600±3) s T=(133±2) K	Arc Observed	Arc Observed	No Arc Observed	3 Arcs	2 Arcs	2 Large Features	6 arcs. No fluorescence. Poor coincidence.
53	E_B=(7000±1) eV J_B=(1.05±0.01) nA/cm^2 Duration=(1000±3) s T=(127±1) K	No Arc Observed	No Arc Observed	No Arc Observed	No Arcs	No data.	2 Large Features	1 small arcs observed. 2 large events resulting in visible damage and blue fluorescence. 2 damage sites.
Au/Cr coated fiberglass and carbon fiber sample, Au side exposed to beam, for IEC radiator baffles								
60	E_B=(22000±1) eV J_B=(1.05±0.01) nA/cm^2 Duration=(3600±3) s T=(165±8) K	Arc Observed	Arc Observed	>16 Arcs	9 Arcs	6 Arcs. 1 Arc/Glow	Extensive multiple damage sites.	>17 total arcs and 1 arc/glow. Very Good Coincidence. Extensive damage sites.
61	E_B=(22000±1) eV J_B=(0.12±0.01) nA/cm^2 Duration=(3600±3) s T=(165±5) K	Arc Observed	Arc Observed	6 Arcs 2 Long Arcs	6 Arcs 2 Long Arcs	2 Arc 2 Glows	Extensive multiple damage sites.	6 arcs and 2 glows. Excellent Coincidence. Extensive damage sites.
62	E_B=(7000±1) eV J_B=(0.12±0.01) nA/cm^2 Duration=(3600±3) s T=(164±7) K	Arc Observed	Arc Observed	No Arcs	No Arcs	No Arcs	Extensive multiple damage sites.	Extensive damage sites.

Table 4.1: Overview of tests 50, 51, 52, 53, 60, 61, and 62.

Induced Electrostatic Breakdown Test Results Overview

Test	Test Parameters	Current Tests			Image Tests			Summary
		Oscilloscope Resistance	Oscilloscope Pearson Coil	Electrometer	Low Light Video	High Res. Still	Microscope Before/After	
IEC Shell Face Sheet with Carbon Veil								
70	E_B=(22000±1) eV J_B=(0.1±0.1) nA/cm^2 Duration=(3600±3) s T=(185± 1) K	3 Arcs	3 Arcs	1 long decay 1 long growth >33 arcs	1 long glow (decays) 19 arcs	1 long decaying glow (brighter in last 3 frames)	No noticeable change.	At least 33 arc events occurred. 1 exp. decaying and 1 exp. growing current observed. No visible damage to sample.
71	E_B=(22000±1) eV J_B=(1.5 ± 0.03) nA/cm^2 Duration=(1000±3) s T=(195± 1) K	2 Arcs	2 Arcs	1 long decay 5 arcs	1 long glow (decays) 1 arc 1 small arc	1 long decaying glow	No noticeable change.	At least 5 arc events occurred. 1 exp. decaying and 1 exp. growing current observed. No visible damage to sample.
72	E_B=(7000±1) eV J_B=(0.1± 0.03) nA/cm^2 Duration=(3600±3) s T=(190± 1) K	1 Arc	1 Arc	No decay No arcs	No glow No arcs	No glow No arcs	No noticeable change.	1 possible arc event. No decaying current. No visible damage to sample.
73	E_B=(7000±1) eV J_B=(1.54 ± 0.03) nA/cm^2 Duration=(1000±3) s T=(200189± 2) K	1 Arc	1 Arc	No decay 2 arcs	2 arcs 1 small arc	Very faint decaying glow	No noticeable change.	At least 2 arc events. No decaying current. No visible damage to sample.
Au Coated Fiberglass IEC Frame								
80	E_B=(22000±1) eV J_B=(1.07 ± 0.03) nA/cm^2 Duration=(1000±3) s T=(126±1) K	No arcs	No arcs	1 exponential decay 1 arc	Not Yet Analyzed	1 long decaying glow	Not Yet Analyzed	At least 1 arc event. 1 exp. decaying current.
81	E_B=(22000±1) eV J_B=(0.14 ± 0.03) nA/cm^2 Duration=(3600±3) s T=(128±1) K	No arcs	No arcs	1 exponential decay 1 arc	Not Yet Analyzed	3 arcs	Not Yet Analyzed	Approx. 3 arc events. 1 exp. decaying current.
82	E_B=(7000±1) eV J_B=(0.25 ± 0.03) nA/cm^2 Duration=(3600±3) s T=(132±2) K	No arcs	No arcs	No arcs	Not Yet Analyzed	≥ 3 arcs	Not Yet Analyzed	Approx. 3 arc events observed only by the still camera. No decaying current.

Table 4.2: Overview of tests 70, 71, 72, 73, 80, 81, and 82.

	Low current *0.1 nA/cm²*	High current *1.0 nA/cm²*	All currents *0.1, 1.0 nA/cm²*
Low energy *7 keV*	0	1	1
High energy *22 keV*	4	4	8
All energies *7, 22 keV*	4	5	9

Table 4.3: Number of experiments in which a glow occurred versus beam energy and beam density.

4.2 IEC Shell Face Sheet with Carbon Veil

A more in-depth discussion of the data acquired and analysis for one material, the IEC Shell Face Sheet with Carbon Veil, is given below. Several discharge events occurred during ESD testing for the IEC Shell material. These events were observed by some or all of the detection instruments. Details of the observations for Tests 70, 71, 72, and 73 follow.

4.2.1 Test 70: E_B=22000 ± 1 eV, J_B=0.1 ± 0.1 nA/cm^2, t=3600 ± 3 s, T=185 ± 1 K

More ESD events occurred during Test 70 than in any of the fourteen tests performed in this study. Evidence of dramatic discharge events was seen in all of the optical and electrical detection methods. An exponentially decaying current beginning at about 600 s was detected by the oscilloscope, electrometer, still camera, and video camera. At least 35 arc events were also detected throughout the experiment.

Electrometer Data for Test 70

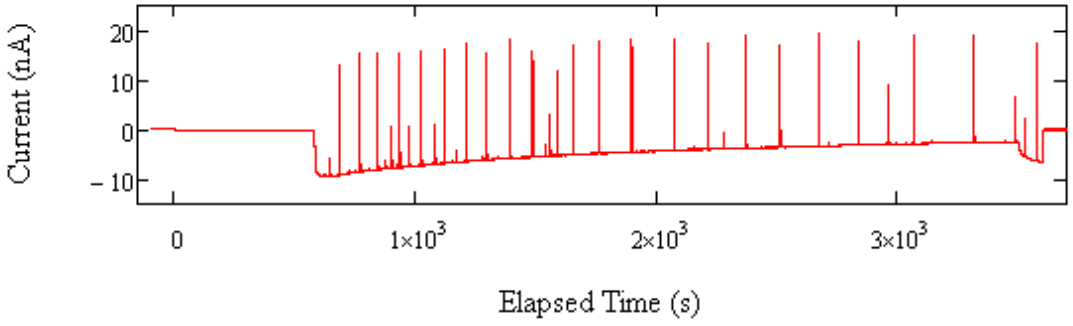

Fig 4.1: Graph of Electrometer Current versus time for Test 70.

The current data recorded by the electrometer provide an excellent overview of the entire test. At approximately 580 s a sudden-onset, exponentially decaying negative current began to flow. It reached a minimum value of -9.47 nA and then decayed toward 0 nA until about 3500 s, after which the current appears to exponentially grow in the negative current direction. After 580 seconds, at least 35 arc signatures appear in the electrometer trace. Table 4.4 summarizes the times and peak values for each of these arcs. Although the sudden-onset, decaying current is negative, the arc events are positive. In other

words, electrons flow in opposite directions for the two phenomena. A summary of arcs, including the time at which they occurred and their peak currents, appears in Table 4.4.

Time Elapsed (s)	Arc Height from Base Current (nA)	Time Elapsed (s)	Arc Height from Base Current (nA)	Time Elapsed (s)	Arc Height from Base Current (nA)
644	3.06	1207	23.68	2275	3.32
681	22.06	1293	21.38	2369	22.65
767	23.82	1390	23.77	2510	20.50
840	23.25	1485	21.23	2670	22.51
872	1.50	1536	2.18	2836	20.87
900	8.32	1557	8.41	2960	11.80
932	22.87	1586	17.19	3065	21.92
972	7.91	1650	22.18	3315	21.69
1021	23.06	1759	22.38	3487	8.97
1074	8.14	1896	22.70	3527	7.91
1116	22.86	2071	22.38	3576	23.74
1167	2.51	2209	21.55		

Table 4.4: Time of occurrence and arc heights for Test 70

Oscilloscope Data for Test 70

The oscilloscope was triggered 621 s, 2070 s, and 3527 s after the electron beam began impinging on the sample surface. The data from the current monitor (PC) and shunt ammeter (Resistor) are in Figures 4.2, 4.3, and 4.4.

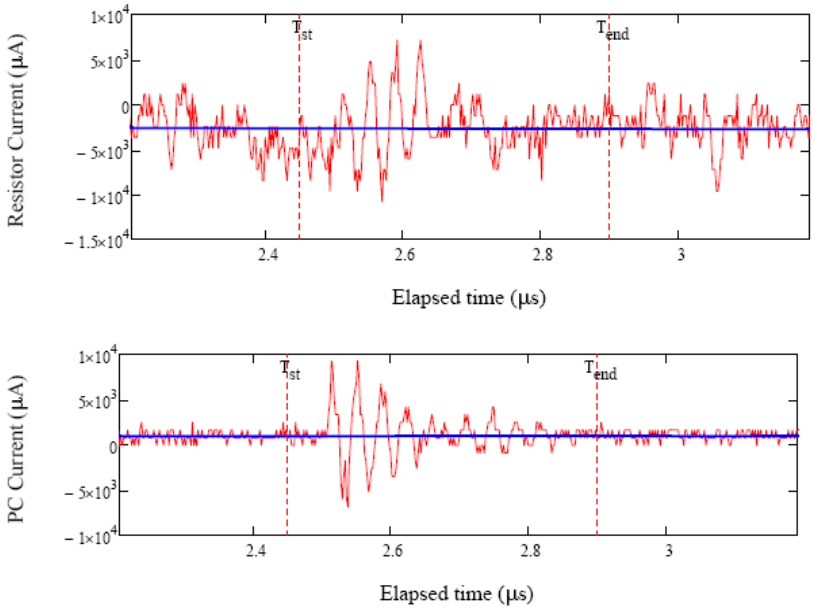

*Fig 4.2: Graphs of Resistor and Pearson Coil (PC) current for Test 70 at **621 s**.*

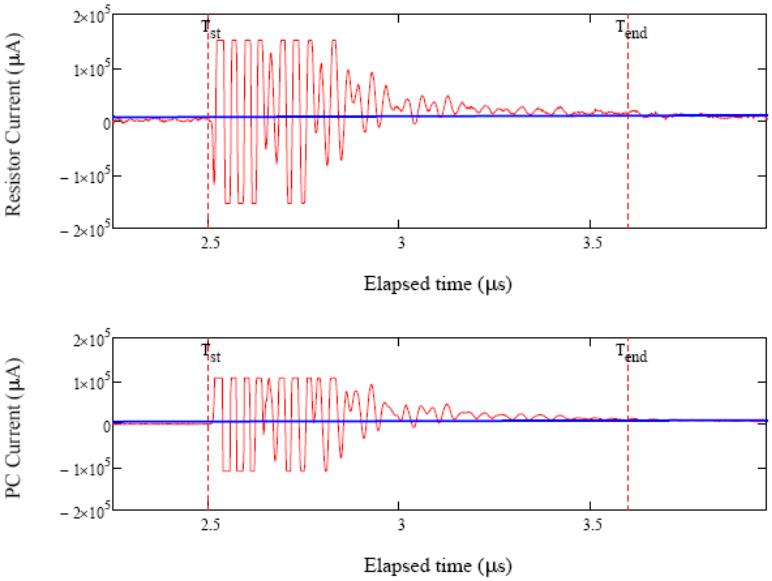

*Fig 4.3: Graphs of Resistor and Pearson Coil (PC) current for Test 70 at **2070 s.***

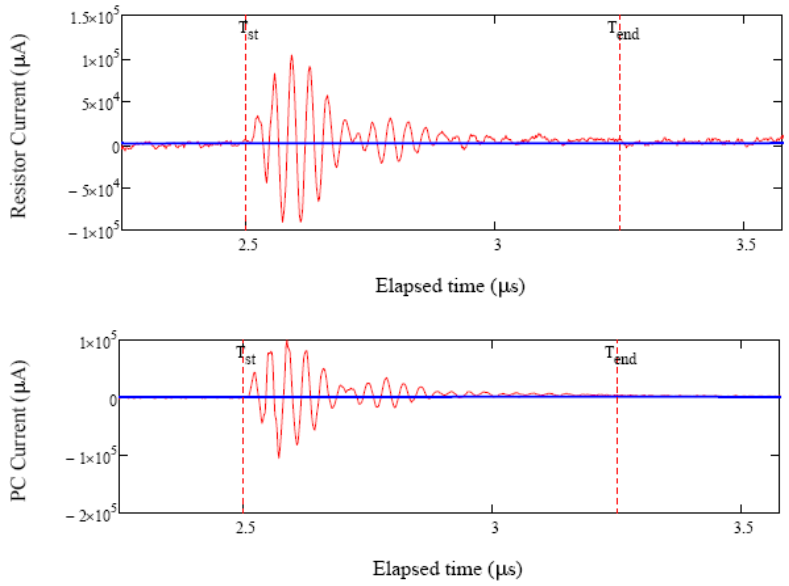

*Fig 4.4: Graphs of Resistor and Pearson Coil (PC) current for Test 70 at **3527 s.***

The energy of each event as recorded by the shunt ammeter or resistor (E_R) and the arc energy recorded by the Pearson Coil (E_{PC}) were calculated by integrating the measured current and multiplying this by the estimated breakdown voltage, 5 V. The breakdown voltage is the product of the breakdown electric field (about 20 MV/m for the epoxy in the IEC Shell material[18]) and the CSDA Range. The calculated arc energy values are listed in Table 4.5. It is interesting to note that these energies span almost three decades in energy.

Event time (s)	E_R (μJ)	E_{PC} (μJ)
621	2.41 ± 0.06	2.14 ± 0.05
2070	> 1189 ± 6	> 1086 ± 5
3527	167 ± 1	181 ± 1

Table 4.5: Arc energies calculated with resistor data (E_R) and Pearson Coil data (E_{PC}).

From the graphs above, it seems that the ESD events occurring at 621 s and 3527 s were completely captured by the oscilloscope. The event at 2070 s was an oscillating current that exceeded the oscilloscope's preset range (± 0.1 A).

It should also be noted that the oscilloscope did not reset automatically after the initial trigger at 621 s. Additionally, there is a time delay after the oscilloscope is triggered—it records the triggered time window of data, then saves this data as a text file, and then begins measuring sample current again. For these reasons, several arc events could have been missed between 621 s and 2070 s, when the oscilloscope was manually reset.

Digital SLR Camera Data for Test 70

The digital still photographs contain evidence of discharging during test 70. These photographs show intensity integrated over 30 seconds and were taken at 34-second time intervals. Beginning with the eighteenth sample frame (i.e. after an elapsed time of about 578 s), a football-shaped region of the sample appears to emit photons. This glow has a sudden onset, and slowly decays in intensity throughout succeeding frames. The glow becomes brighter in the last three sample frames, 104-106. (Frame 107 was likely taken after the electron beam was turned off.)

It is likely that this phenomenon is related to the sudden increase in sample current, which also slowly decays over time. The decrease in base sample current near the end of the test seems to correlate with the increased brightness of the glow in the last few frames.

There is also a very faint glow seen in frames 1 through 17, which correlates with the electron beam turning on.

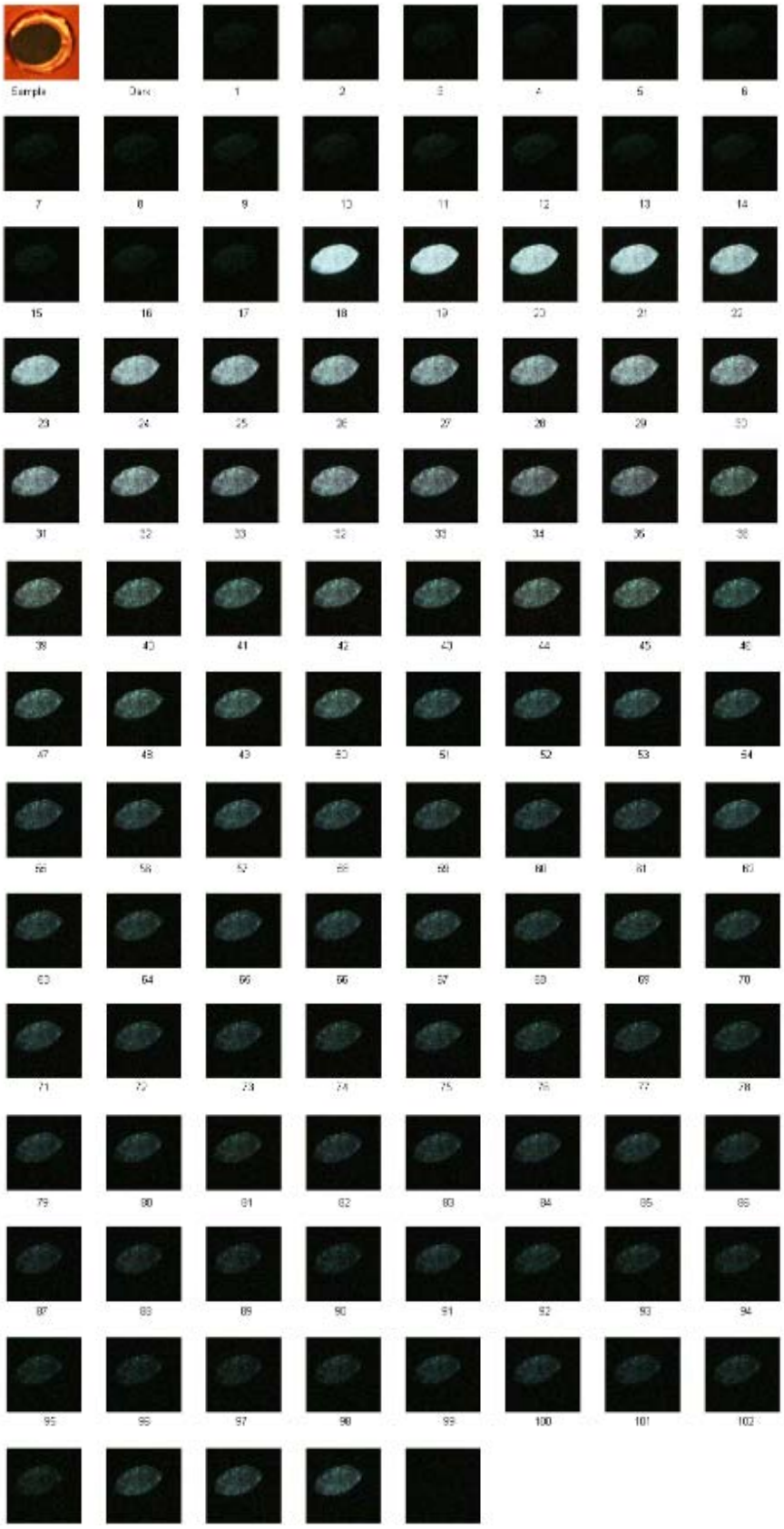

Fig 4.5: Photographs taken by Digital SLR Camera for Test 70. Sample: Image taken in full light. Dark: 30-second exposure taken with all light sources off. 1-107: 30-second exposures taken consecutively during Test 70 with a four-second reset time between frames.

The relative intensity of each frame was used to create the graph of integrated arc intensity and arc energy shown below. Again notice the sudden increase in intensity at approximately 600 s and the gradual intensity increase beginning at about 3500 s. The linear nature of the semi-log curve suggests exponential intensity decay.

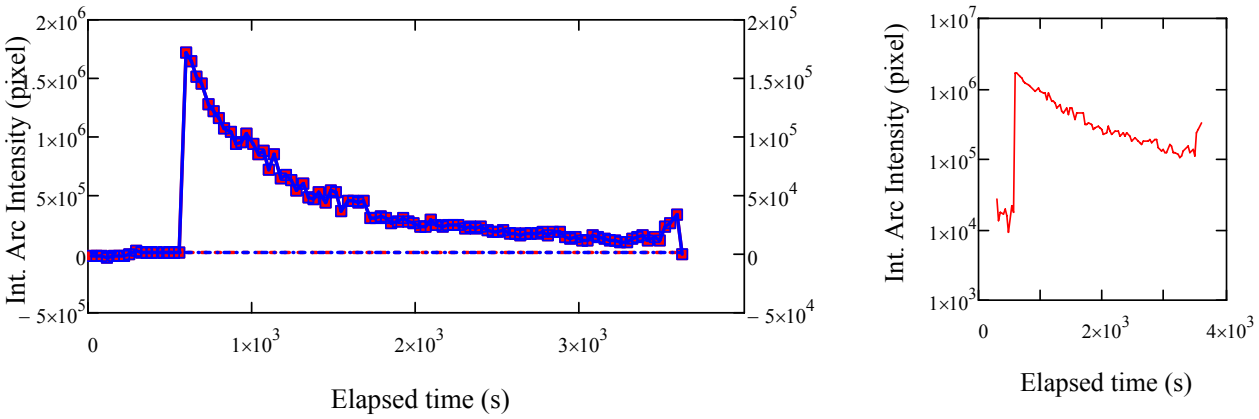

Fig 4.6: Intensity of Test 70 still camera images versus time. a) linear plot b) semi-log plot.

No sudden flashes or arc events appear in the digital photographs. The arcs detected by the electrometer may have produced a sudden flash of photons, but the exponentially-decaying glow seen after 578 s masked any arcing events that may have taken place.

Low-level Video Camera Data for Test 70

The low-level video camera detected the decaying glow as seen in the still camera photographs, and was also able to detect arc events. A small flash, which may have been an ESD event, was detected at 376 s. The sudden luminescence was first seen at 580 seconds, after which it slowly decreased in brightness. This glow was still present during the succeeding arc events, which were characterized by a sudden flash or increase in light intensity. These arc events occurred at 643, 680, 767, 899, 932, 1115, 1207, 1294, 1390, 1558, 1589, 1650, 1760, 1897, 2071, 2671, 2961, 3015, and 3316 seconds.

Microscope Imaging Results for Test 70

As shown to the right, from a macroscopic view, it is difficult to notice any discrepancies between the sample surface before and after ESD testing. Careful inspection under a microscope also confirmed that no noticeable change between the sample surface before and after ESD testing.

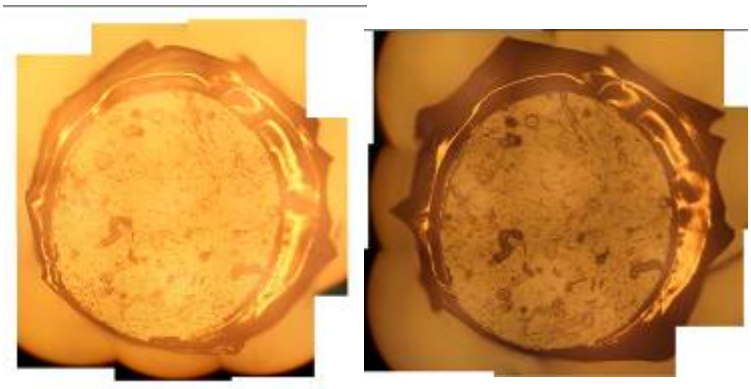

Fig 4.7: High resolution image of sample 70 a) before ESD testing and b) after ESD testing.

4.2.2 Test 71: E_B=22000±1 eV, J_B=1.5 ± 0.03 nA/cm^2, t=1000±3 s, T=195± 1 K

A higher flux density was used during this test, but the duration was shorter. A sudden-onset exponentially-decaying current was first detected at about 600 seconds. At least five additional arc events were also observed.

Electrometer Data for Test 71

The data recorded by the electrometer shows a sudden-onset, exponentially-decaying current similar to that seen in Test 70. Five arc events were also detected, the first of which appears to have happened either immediately before or simultaneously with the onset of the exponentially-decaying current. This arc occurred at 572 s, and is a spike in the negative current direction with a peak value of -15.75 nA from the base current. The other arcs (at 645, 781, 924, and 954 s) occur after the sudden-onset current, and are spikes in the direction of positive current.

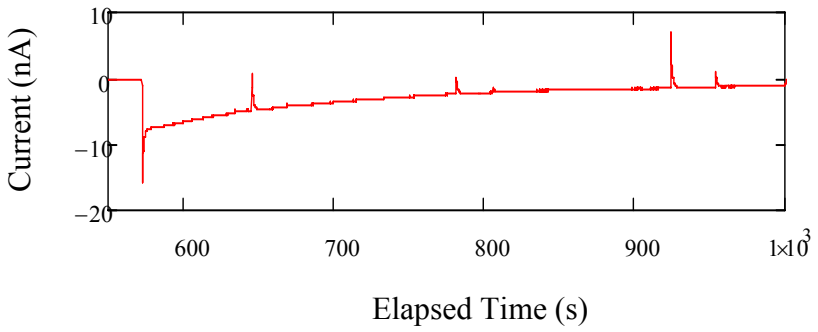

Fig 4.8: Graph of Electrometer Current versus time for Test 71.

Time Elapsed (s)	Arc Height from Base Current (nA)
572	-15.75
645	5.73
781	2.53
924	8.42
954	2.39

Table 4.6: Time of occurrence and arc heights for Test 71.

Oscilloscope Data for Test 71

Although the oscilloscope was triggered four times during the experiment, it appears that the first two triggers were invalid as the data recorded is of a completely different time scale from the time scale set for ESD triggering. The last two pulses, occurring at 924 s and 954 s, have the right time scale. Graphs of resistor and Pearson Coil currents versus time, as well as the energies of these events are shown in Figures 4.9 and 4.10 and Table 4.7.

Event time (s)	E_R (µJ)	E_{PC} (µJ)
924	124 ± 2	135 ± 1
954	9.1 ± 0.3	13.4 ± 0.3

Table 4.7: Test 71 arc energies calculated with resistor data ($\mathbf{E_R}$) and Pearson Coil data ($\mathbf{E_{PC}}$).

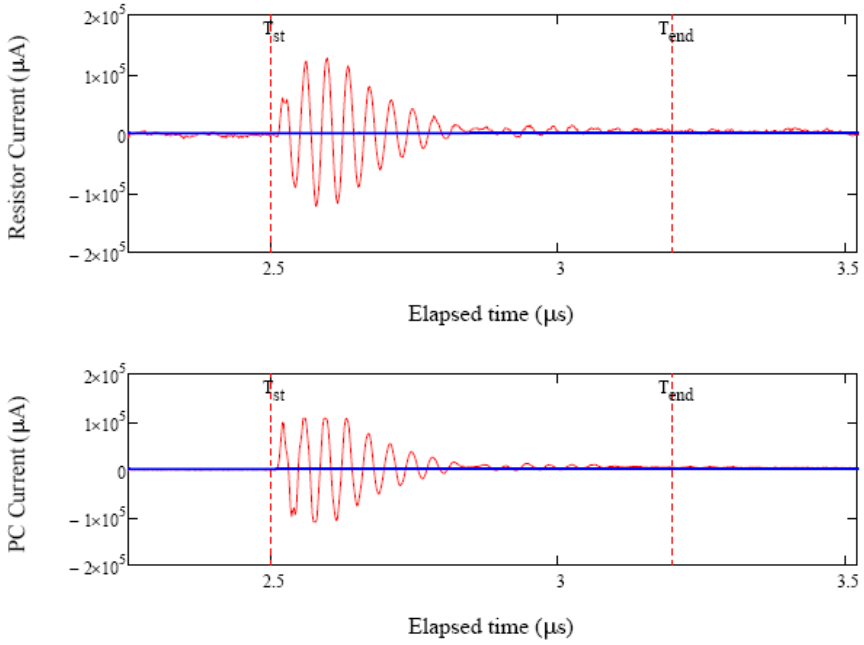

*Fig 4.9: Graphs of Resistor and Pearson Coil (PC) current for Test 71 at **924 s**.*

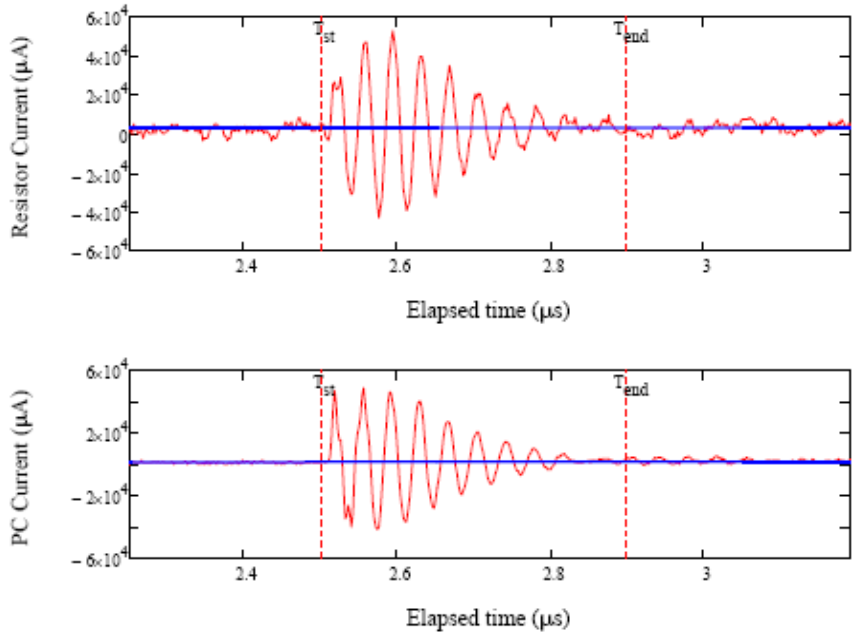

*Fig 4.10: Graphs of Resistor and Pearson Coil (PC) current for Test 71 at **954 s**.*

Digital SLR Camera Data for Test 71

A sudden-onset luminescence appears near the end of Frame 17 and the beginning of frame 18, at approximately 575 seconds. The glow gradually decreases until the beam is turned off at the end of the last frame. Like Test 70, there is also a very faint glow seen in frames 1 through 17, which correlates with the electron beam turning on. Also as with the photographs for Test 70, no arcs/flashes were observed, probably due to the light from the luminescence overpowering any quick events that may have occurred.

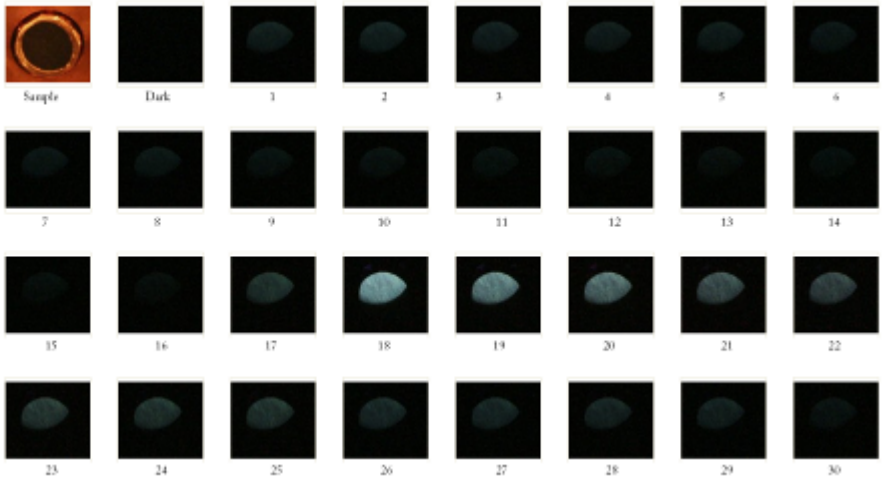

Fig 4.11: Photographs taken by Digital SLR Camera for Test 71. Sample: Image taken in full light. Dark: 30-second exposure taken with all light sources off. 1-30: 30-second exposures taken consecutively during Test 70 with a four-second reset time between frames.

Low-level Video Camera Data for Test 71

A very small flash observed at 284 s may have been ESD-related. The flash was close in magnitude to the background noise of the video frames, however, and could have been noise. A decaying glow began at 573 s and a flash, indicating an arc, occurred at 924 s.

Microscope Imaging Results for Test 71

No noticeable changes were observed between the sample surface before and after Test 71, as shown in Figure 4.12.

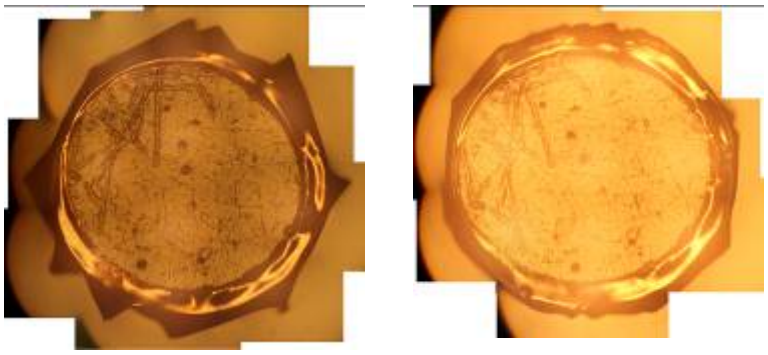

Fig 4.12: High resolution image of sample 71 a) before ESD testing and b) after ESD testing.

4.2.3 Test 72: *E_B=7000±1 eV, J_B=0.1± 0.03 nA/cm^2, t=3600±3 s, T=190± 1 K*

Electrometer Data for Test 72

No arcs or persistent exponentially decaying currents were observed by the electrometer during test 72 (see Figure 4.13), which had a lower electron beam energy (E_B = 7000±1 eV) than tests 70 and 71 (E_B = 22000±1 eV) and had a current flux density, J_B=0.1± 0.03 nA/cm^2.

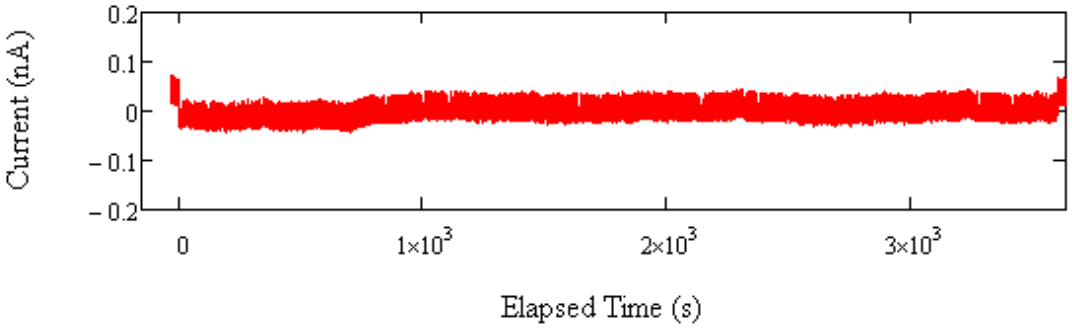

Fig 4.13: Graph of Electrometer Current versus time for Test 72.

Oscilloscope Data for Test 72

The oscilloscope was only triggered once during test 72 at 1399 seconds. Figure 4.14 shows the oscilloscope traces. The energy of the arc was 1.6 ± 0.1 µJ as recorded by the resistor and 0.45 ± 0.02 µJ as measured by the Pearson Coil.

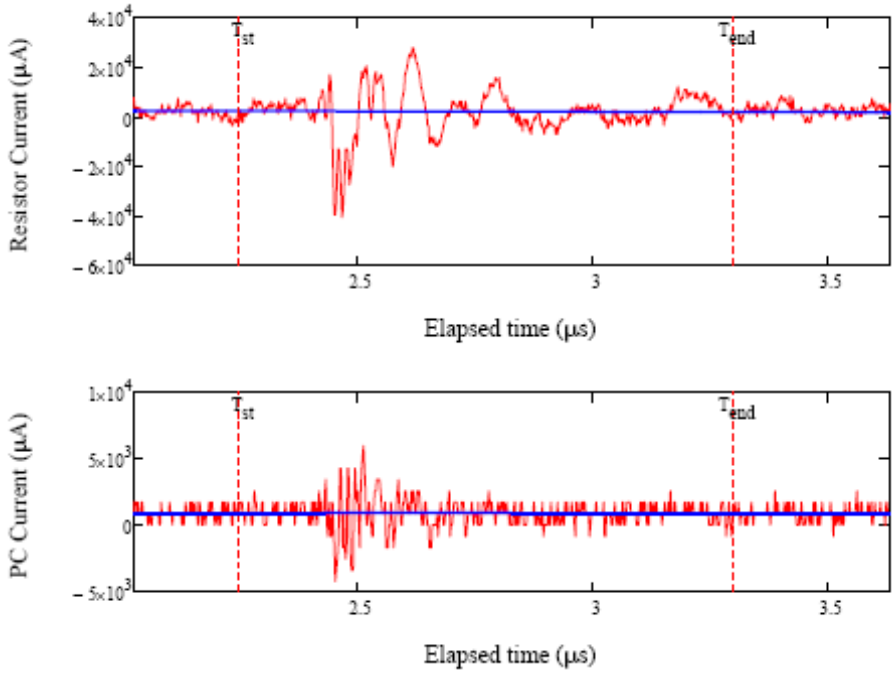

*Fig 4.14: Graphs of Resistor and Pearson Coil (PC) current for Test 72 at **1399 s.***

Digital SLR Camera Data for Test 72

No arcing or persistent glows were detected by the digital still camera. All of the 107 frames taken during experimentation look like the dark image. The first 30 of these frames are in Figure 4.15.

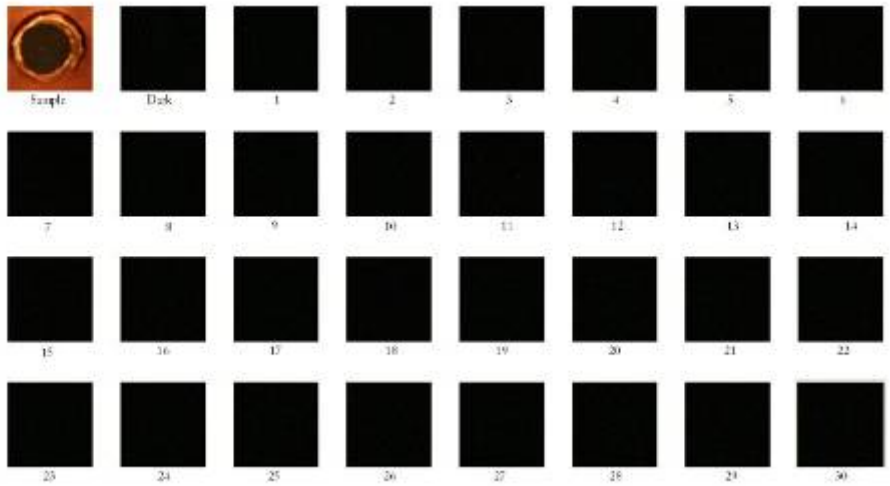

Fig 4.15: Photographs taken by Digital SLR Camera for Test 72. Sample: Image taken in full light. Dark: 30-second exposure taken with all light sources off. 1-30: 30-second exposures taken consecutively during Test 70 with a four-second reset time between frames.

Analysis of the light intensity of each frame is also shown in Figure 4.16. As the intensity never rises above the minimum detectable intensity (or noise threshold), no significant light flashes or glows occurred during this test.

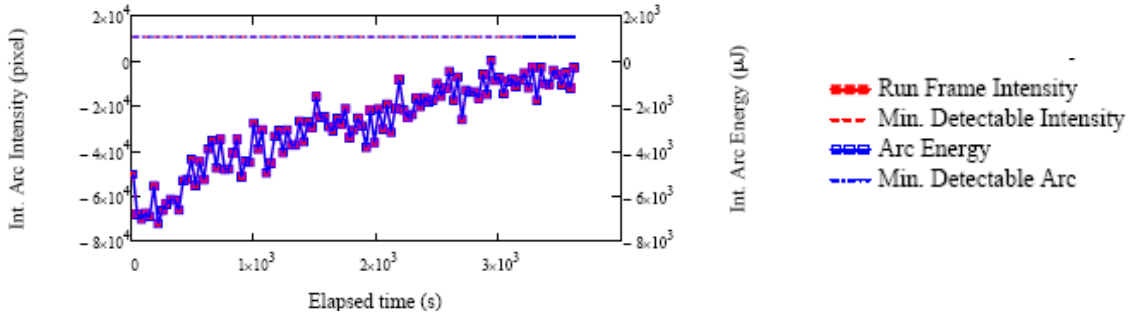

Fig 4.16: Intensity of Test 72 still camera images versus time.

Low-level Video Camera Data for Test 72

No glows or flashes were detected by the low-level video camera during this test.

Microscope Imaging Results for Test 72

No noticeable changes were observed between the sample surface before and after Test 72 (see Fig. 4.17).

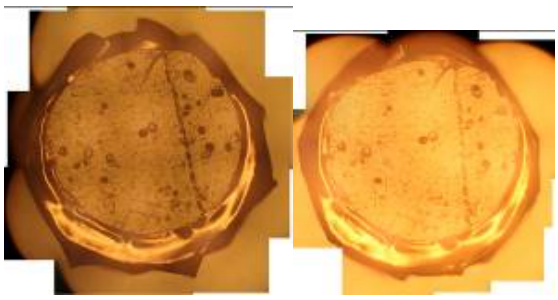

Fig 4.17: High resolution image of sample 72 a) before ESD testing and b) after ESD testing.

4.2.4 Test 73: E_B=7000±1 eV, J_B=1.54 ± 0.03 nA/cm^2, t=1000±3 s, T=200189± 2 K

Electrometer Data for Test 73

As for test 72, no exponentially-decaying currents appear in the electrometer data for Test 73. However, two small arc events were detected at t = 804s and t = 944 s, which reached peak values of I = 0.16 nA and I = 0.29 nA, measured from the baseline current. (See Table 4.8 and Figure 4.18.)

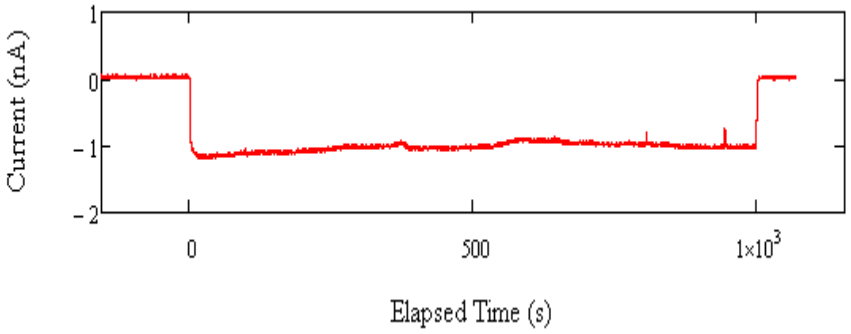

Time Elapsed (s)	Arc Height from Base Current (nA)
804	0.16
944	0.29

Table 4.8: Time of occurrence and arc heights for Test 73.

Fig 4.18: Graph of Electrometer Current versus time for Test 73.

Oscilloscope Data for Test 73

The oscilloscope was also triggered at 945 seconds, which corresponds in time with a small arc observed in the electrometer data. The energy of the arc was 1.46 ± 0.01 μJ as recorded by the resistor and 0.242 ± 0.008 μJ as measured by the Pearson Coil. Figure 4.19 shows the resistor and Pearson Coil currents during the event.

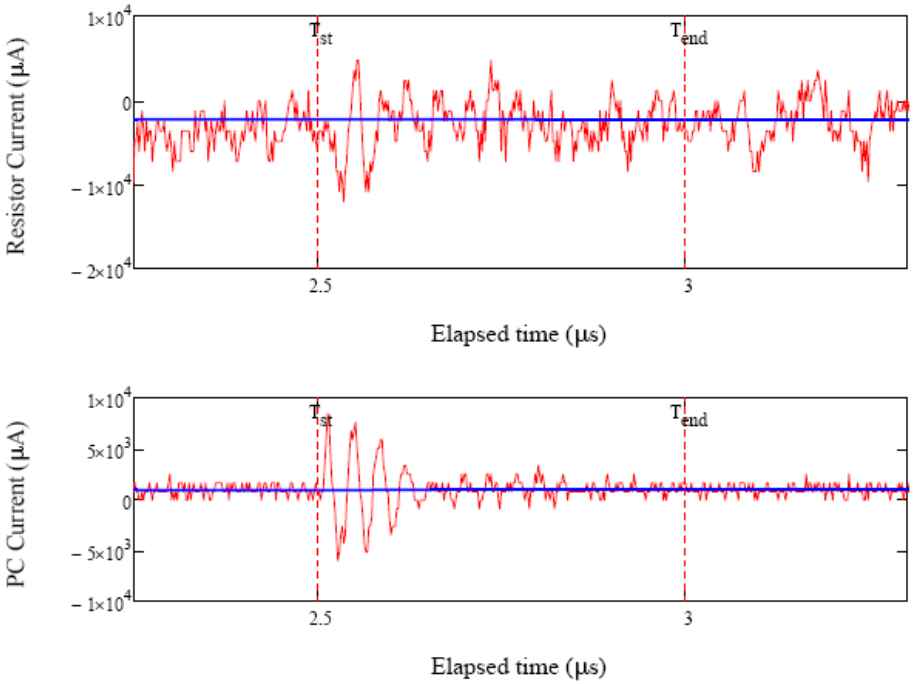

*Fig 4.19: Graphs of Resistor and Pearson Coil (PC) current for Test 73 at **945 s**.*

Digital SLR Camera Data for Test 73

A very faint decaying glow can be seen in the frames throughout the experiment (see Figure 4.20). Similar phenomena are observed at the beginning of Tests 70 and 71.

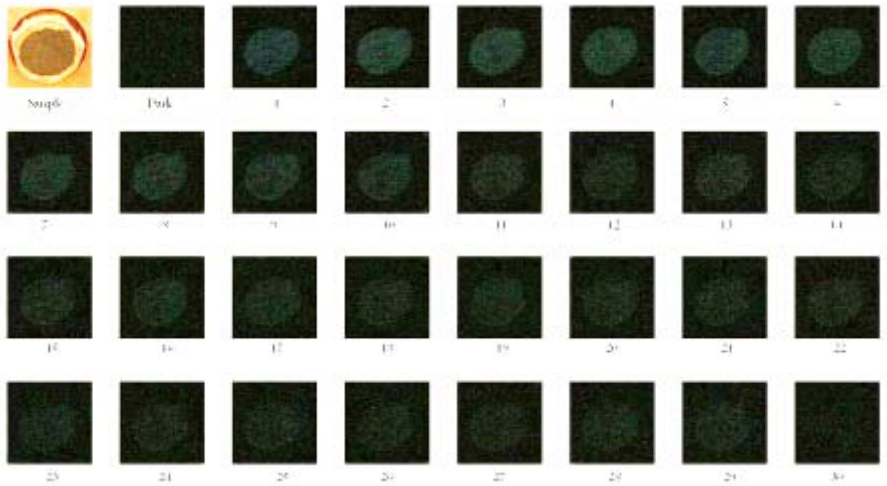

Fig 4.20: Photographs taken by Digital SLR Camera for Test 73. Sample: Image taken in full light. Dark: 30-second exposure taken with all light sources off. 1-30: 30-second exposures taken consecutively during Test 70 with a four-second reset time between frames.

Low-level Video Camera Data for Test 73

Three possible arcing events were captured by the video camera during Test 73. One small flash at 166 s was only slightly brighter and larger than the background noise; it suggests ESD may have occurred, but is not compelling evidence. Two distinct flashes at 801s and 941 s provide stronger indications that ESD occurred. Both flashes correspond to times for arcs seen in the electrometer data.

Microscope Imaging Results for Test 73

No noticeable changes were observed between the sample surface before and after Test 72, as shown in Figure 4.21.

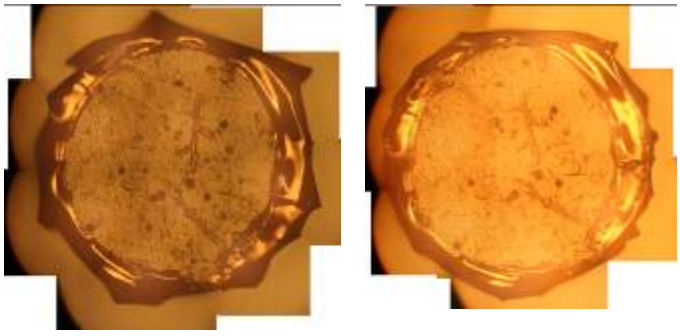

Fig 4.21: High resolution image of sample 73 a) before ESD testing and b) after ESD testing.

CHAPTER 5
CONCLUSIONS

Although further analysis is necessary before any definitive conclusions can be reached, there is evidence that electrostatic discharge can be induced by the conditions of electrons in the L2 space plasma environment. Discharge events occurred for all four materials under the simulated accelerated space plasma charging conditions. ESD events occurred for all eight experiments using the higher energy electron beam (~22 keV), whereas only one of the six lower energy (7 keV) electron beam tests induced ESD. Five of the six higher current (1.0nA/cm^2) beams induced glows, while glows occurred for only four of the eight lower current (0.1 nA/cm^2) experiments (see Table 4.3).

Two types of discharge events were observed: a sudden-onset, persistent, exponentially-decaying current accompanied by luminescence and a brief spike, or arc, in current sometimes accompanied with a flash in the video data. For the gold-covered samples, any glows seen occurred around the edge of the sample. For the composite materials, glows occurred in a football shape across about one-third of the sample surface. The initial magnitude of the glow current ranged from 1.7 times the electron beam current, to 121 times the electron beam current. The still camera and electrometer showed exponential decays with time constants on the order of 10 minutes. Multiple glows did occur in some cases. In all five experiments where the glow extended to the end of testing, the glow ceased immediately when the beam turned off. The coincidence of glows was very good between electrometer, video, and still camera data.

Analysis of the oscilloscope data showed that the arcs had periods on the order of 0.05 μs and lasted for about 1 μs. These events had energies ranging from 0.02 μJ to 1200 μJ, and reached maximum currents of 5.1 to 181 mA. In four of the five tests where arcs occurred outside of a glow, these arc currents were negative. For all five tests with arcs occurring during a glow, these arc currents were positive. Sometimes the oscilloscope would not trigger for an arc detected by the other two methods. However, there was good overall coincidence of arcs between electrometer, oscilloscope, and video data.

The results of this study have already initiated a project by the JWST design team to increase the thickness of the conducting gold layer of the IEC Au Radiator Reflector Material. This is intended to mitigate arcing induced by storm conditions in the L2 environment. Based on the estimation that approximately 2% of the gold surface was removed during irradiation by the electron beam, JWST researchers are considering the feasibility of increasing the thickness of the gold layer to enhance charge

dissipation and reduce the likelihood of exposing the underlying fiberglass and carbon fiber material. Additional design alterations may also be necessary for all materials to avoid ESD anomalies, particularly to minimize light contamination from glows.

Future research at USU includes further analysis of data already taken. This analysis includes, but is not limited to: determination of arc energy as measured by the electrometer, calculating time constants for the exponentially decaying currents, computation of accumulated charge at onset time for exponentially decaying currents, analysis of comparative brightness of video frames, and determining the orientation and magnitude of luminescence on video and still camera shots. It would also be beneficial to perform more precise sensitivity measurements for each of the detection instruments to better understand the limitations of each detection method.

Additional planned experimentation would involve incorporating a spectrometer into the ESD detection system, in order to better characterize the luminescence or glow seen in many of the tests. Using a phosphor screen to characterize the shape of the electron beam may provide explanations for the shape of the glow, which has an abrupt edge in the upper left portion of each sample. There are also plans to exactly repeat several ESD tests, which will provide information about the reproducibility of arc events. Future testing will be performed for the Au Radiator Reflector material with a thicker layer of gold to test the functionality of the thicker gold layer.

REFERENCES

[1] L. Tyahla, "The Hubble Space Telescope Project," <http://hubble.nasa.gov/> (Dec. 2008).

[2] D.P. Stern, "Lagrangian Points," NASA Educational Website, <http://www-istp.gsfc.nasa.gov/Education/wlagran.html> (Mar. 2006).

[3] J.P. Gardner, *et al.,* "The James Webb Space Telescope," Space Sci. Rev. **123**, 485 (2006).

[4] D.J. Mount, "Thin Films and MEMS Devices Enable the JWST Space Telescope," Vac. Tech. Coat. Mag., 50 (Aug. 2007).

[5] J.R. Fennell, H.C. Koons, J.L. Roeder, and J.B. Blake, "Spacecraft Charging: Observations and Relationship to Satellite Anomalies," 7th International SCTC, Noordwijk Netherlands, (Apr. 2001).

[6] R. Hoffmann, et al., "Low-Fluence Electron Yields of Highly Insulating Materials," IEEE Trans. on Plasma Science, Vol **36**, No 5 (2008).

[7] J.I. Minow, et al., "Plasma Environment and Models for L2," 42 AIAA Aero. Sci. Mtg., Reno NV, (Jan. 2004).

[8] R.D. Leach and M.B. Alexander, "Failures and Anomalies Attributed to Spacecraft Charging," NASA Ref. Pub. 1375, NASA Marshall Space Flight Center, (Aug. 1995.)

[9] N. W. Ashcroft and N. D. Mermin, "Solid State Physics," USA.: Thomas Learning, 223, (1976).

[10] B.F. James, O.W. Norton, and M.B. Alexander, "The Natural Space Environment: Effects on Spacecraft," NASA Ref. Pub. 1350, NASA Marshall Space Flight Center, (Nov. 1994.)

[11] C.J. Tung and C.M. Kwei, "CSDA Ranges of Electrons in Metals," Chin. Jour. Phys., Vol **17**, No 1 (1979).

[12] J.A. Roth, J.R. Dennison, R. Hoffmann, "Observation and Characterization of Electrostatic Discharge in Insulating Materials Induced by Electron Beam Bombardment," APS 4CS Mtg., El Paso TX, (Oct. 2008).

[13] J.R. Dennison, "JWST IEC/ICIM Sample Induced Electrostatic Breakdown Tests," USU Surf. Phys., (Mar. 2009).

[14] H.A. Strobel and W.R. Heineman. *Chemical Instrumentation: A Systematic Approach*, 3rd Edition, New York USA: Wiley, 516, (1989).

[15] D. C. Ferguson *et al*., "NASA GRC and MSFC Space Plasma Arc Testing Procedures," IEEE Trans. on Plasma Science, Vol **34**, No 5 (2006).

[16] S.H. Voldman, "ESD: Physics and Devices," Hoboken, USA: Wiley, 5, (2004).

[17] V. Zavylov, "Ammeter Report," USU Surf. Phys., (circa 2000).

[18] W. Tillar Shugg, *Handbook of Electrical and Electronic Insulating Materials*, 2nd Ed, Wiley IEEE Press, (1995).

AUTHOR'S BIOGRAPHY

Jennifer Albretsen Roth was born in Lafayette Indiana. She graduated from Waunakee High School in Wisconsin in the spring of 2005, and has been attending Utah State University since the fall of 2005. During her time at USU she has participated in various research projects including: Bear Lake Observatory Riometer (under the direction of Dr. Jan Sojka), X-Ray Diffraction for Hydrogen Storage Material (under the direction of Dr. Leijun Li), Photoyields of Spacecraft Materials, and Electron-Induced Electrostatic Discharge for Spacecraft Materials (both under the direction of Dr. J.R. Dennison). During the summer of 2006, Jennifer studied nanocrystalline copper with Dr. Ian Baker during a Research Experience for Undergraduates at Dartmouth College. She also enjoyed teaching introductory physics labs and leading introductory physics recitations during her undergraduate career. She and her husband, Gable, look forward to beginning graduate studies at Oregon State University next fall.